



In vivo study of magnesium plate and screw degradation and bone fracture healing



Amy Chaya^{a,b,d}, Sayuri Yoshizawa^{a,c}, Kostas Verdelis^{a,c,d}, Nicole Myers^{a,c}, Bernard J. Costello^{a,d,e}, Da-Tren Chou^{a,b,d}, Siladitya Pal^b, Spandan Maiti^b, Prashant N. Kumta^{a,b,c,d}, Charles Sfeir^{a,b,c,d,*}

^aThe Center for Craniofacial Regeneration, University of Pittsburgh, Pittsburgh, PA, USA

^bDepartment of Bioengineering, University of Pittsburgh, Pittsburgh, PA, USA

^cDepartment of Oral Biology, University of Pittsburgh, Pittsburgh, PA, USA

^dThe McGowan Institute for Regenerative Medicine, University of Pittsburgh, Pittsburgh, PA, USA

^eDepartment of Oral and Maxillofacial Surgery, University of Pittsburgh, Pittsburgh, PA, USA

ARTICLE INFO

Article history:

Received 18 August 2014

Received in revised form 10 February 2015

Accepted 13 February 2015

Available online 21 February 2015

Keywords:

Magnesium

Fixation devices

Fracture fixation

MicroCT

ABSTRACT

Each year, millions of Americans suffer bone fractures, often requiring internal fixation. Current devices, like plates and screws, are made with permanent metals or resorbable polymers. Permanent metals provide strength and biocompatibility, but cause long-term complications and may require removal. Resorbable polymers reduce long-term complications, but are unsuitable for many load-bearing applications. To mitigate complications, degradable magnesium (Mg) alloys are being developed for craniofacial and orthopedic applications. Their combination of strength and degradation make them ideal for bone fixation. Previously, we conducted a pilot study comparing Mg and titanium devices with a rabbit ulna fracture model. We observed Mg device degradation, with uninhibited healing. Interestingly, we observed bone formation around degrading Mg, but not titanium, devices. These results highlighted the potential for these fixation devices. To better assess their efficacy, we conducted a more thorough study assessing 99.9% Mg devices in a similar rabbit ulna fracture model. Device degradation, fracture healing, and bone formation were evaluated using microcomputed tomography, histology and biomechanical tests. We observed device degradation throughout, and calculated a corrosion rate of 0.40 ± 0.04 mm/year after 8 weeks. In addition, we observed fracture healing by 8 weeks, and maturation after 16 weeks. In accordance with our pilot study, we observed bone formation surrounding Mg devices, with complete overgrowth by 16 weeks. Bend tests revealed no difference in flexural load of healed ulnae with Mg devices compared to intact ulnae. These data suggest that Mg devices provide stabilization to facilitate healing, while degrading and stimulating new bone formation.

© 2015 Acta Materialia Inc. Published by Elsevier Ltd. All rights reserved.

1. Introduction

Each year there are over 6 million bone fractures reported in the U.S. [1], approximately one third of which require internal fixation devices to help facilitate healing [2]. Currently, permanent and inert metals like titanium (Ti) alloys and stainless steel remain the gold standard for internal fixation devices; however, these materials are associated with various long-term complications such as interference with skeletal growth (particularly for pediatrics), tissue irritation, infection, interference with radiological imaging, and unfavorable esthetics (primarily for craniofacial

implants) [3–7]. For these reasons, permanent fixation devices may necessitate invasive removal surgeries, increasing patient burden and risk, and draining valuable hospital resources [8,9]. To mitigate these concerns, resorbable polymer devices have been developed; however their mechanical properties often limit them as viable options for load-bearing applications [10]. Furthermore, studies have reported long-term foreign body reactions associated with polymeric device degradation, likely due to their acidic degradation products [3,11,12]. For these reasons, there remains a need to develop novel fracture fixation devices which mitigate long-term complications and eliminate the need for removal surgeries.

Unlike permanent metals and resorbable polymers, degradable magnesium (Mg) alloys provide a unique combination of strength and degradation. For these reasons, Mg alloys are being explored for various craniofacial and orthopedic applications. Interestingly,

* Corresponding author at: 3501 Terrace St., 598 Salk Hall, Pittsburgh, PA 15261, USA. Tel.: +1 412 648 8500; fax: +1 412 624 6685.

E-mail address: csfeir@pitt.edu (C. Sfeir).

Mg alloys were first attempted as orthopedic devices over a century ago. Early Mg-based devices proved to be biocompatible, with low rates of infection; however, rapid degradation of Mg that is characteristic and to be expected with the current metallurgical knowledge known to date caused excessive hydrogen gas formation which ultimately prevented their clinical success [13,14]. Since these initial investigations, numerous advancements in alloying and corrosion control have been achieved. These advancements allow Mg and its alloys to be tailored to accommodate the desired mechanical properties and degradation behavior.

Numerous *in vitro* and *in vivo* studies have demonstrated the biocompatibility and osteoconductivity of these materials. Indirect assays, in which cells are exposed to media treated with Mg corrosion products, have shown cell viability with low concentrations of degradation product [3,13,15]. Similarly, direct assays, in which cells are cultured directly on Mg alloys, have shown cytocompatibility in the presence of ongoing Mg degradation [3,13,15]. Importantly, studies assessing Mg implants in endosseous sites, such as guinea pig [16], rat [17], and rabbit femora [18] have shown biocompatibility and normal foreign body response for various Mg alloys. In addition, several studies have shown high mineral apposition rates and increased bone mass and mineral density surrounding Mg implants in bone [10,16,19,20].

These data support the use of Mg implants as orthopedic devices; however there remains a lack of *in vivo* data assessing these materials as actual fixation plates and screws. For these reasons, we previously conducted a pilot study to evaluate Mg fixation plates and screws using a rabbit ulna fracture model [21]. In the pilot study, we compared 99.9% Mg plates and screws to clinically-used Ti devices, studying the effect of Mg degradation on fracture healing. Our pilot study results showed no significant difference in healing of fractures fixed with Mg or Ti devices. Interestingly, we also observed bone formation above the Mg, but not Ti, plates and screws.

In order to validate this pilot study data, we have conducted a more thorough follow-up assessment presented herein. In the present study, we aim to test our hypothesis that ongoing Mg device degradation will continue to stimulate osteogenic differentiation of local cell populations such as human bone marrow stromal cells (hBMSCs) and/or periosteal cells. In turn, this differentiation will result in local bone formation, providing additional fracture stabilization. Through this process, it is anticipated that Mg devices will be gradually replaced by bone growth, mitigating risk of long-term complications and device removal surgeries. To test this hypothesis, we have performed a thorough assessment of the degradation behavior and biological effect of Mg fixation devices. Specifically, we have designed and tested Mg fixation plates and screws in a rabbit ulna fracture model. Our results have confirmed our pilot study observations of new bone formation around Mg devices, especially above the devices where the periosteum and muscle tissue was present. In addition, we observed no inhibition of fracture healing. Mechanical testing demonstrated that healed fractures fixed with Mg devices responded similarly to healthy controls when subjected to three point bending. Taken together, these data demonstrate the efficacy of Mg fixation devices in a load bearing fracture site.

2. Materials and methods

2.1. Device design and development

Fixation devices (Fig. 1) were machined with 99.9% pure Mg (Goodfellow, Coraopolis, PA). All devices were designed to accommodate rabbit ulnar geometry. Plates were 20 × 4.5 mm with a thickness of 1–1.5 mm. Screws were 7 mm in length, with a shaft

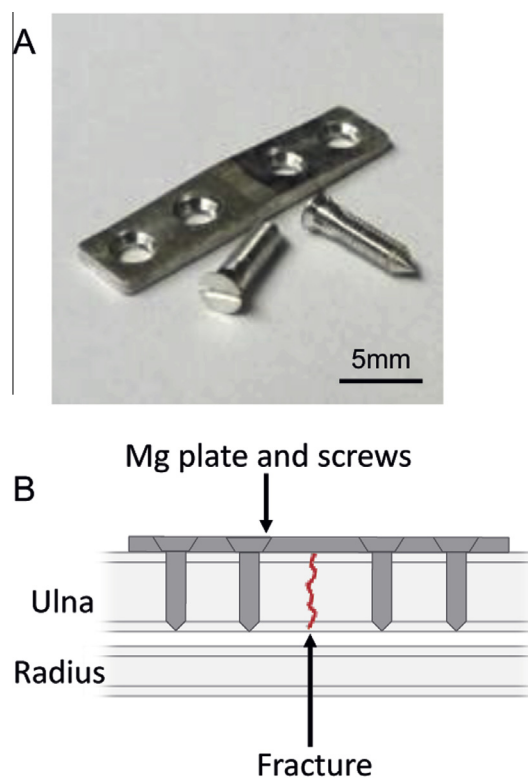


Fig. 1. Magnesium fixation plate and screws. Digital image showing devices prior to implantation (A). Schematic showing device placement with fractured ulna (B).

outer diameter of 1.75 mm and shaft inner diameter of 1 mm. Prior to implantation, devices were cleaned by sonicated washes in pure acetone and ethanol, followed by sterilization with gamma radiation (2×10^6 cGy, 23.5 Gy/min, cesium 137 source, Mark 1 68, JL Shepherd and Associates, San Fernando, CA).

2.2. *In vivo* implantation

All animal experiments were approved by the University of Pittsburgh's Institutional Animal Care and Use Committee. 12 New Zealand White rabbits (19 weeks of age, 3.5 ± 0.2 kg) were used in this study. Both ulnae (right and left) of all animals were used, providing a total of 24 surgical sites. Each time point consisted of 6 rabbits (12 surgical sites). Prior to surgery, animals were anesthetized and forearms were shaved and disinfected. A 2 cm incision was made over the ulna. Overlying skin and muscle was carefully retracted to expose the ulna. A complete ulnar osteotomy (0.5–1 mm thick) was created using a hand held drill. A fixation device consisting of one plate and four screws was then placed to stabilize the fracture. The incision was closed in layers with sutures and left un-casted. Animals were monitored daily for general behavior, movement, and food and water intake. In addition, forearms were checked thoroughly by visual inspection and gentle palpation for signs of infection or subcutaneous gas pocket formation. Based on consultation with the University of Pittsburgh's Division of Laboratory Animal Resources, observable gas pockets were removed with a sterile syringe. All gas pocket formations and removals were documented throughout the study.

2.3. X-ray imaging

X-ray imaging was used to monitor device placement and fracture healing throughout the study. All animals received X-rays immediately following surgery and every 2 weeks thereafter.

2.4. Three point bend test

A three point bend test was used to evaluate the relative strength of the ulnae after 16 weeks ($n = 9$ ulnae). Prior to testing, forearms were carefully dissected and overlying soft tissue was removed. For all samples, the radius and ulna were fused, preventing us from accurately separating the bones for testing. To exclude radial contributions from the test, two transverse cuts were created on either side of the fracture site and remaining device (4 cm apart) using a low speed saw and diamond blade (Buehler USA, Lake Bluff, IL) as previously described [22]. An Instron 5564 (Instron USA, Norwood, MA) with 2 kN load capacity was used for testing. For each sample, the radius and ulna were positioned on the same horizontal plane on two lower stabilizing points positioned 5 cm apart. The fracture site and radial cuts were centered within these points. One upper moving point was positioned at the center of the two lower points. Test parameters were modified from previous studies, including a 1 N pre-load, loading speed of 5 mm/min, and stop point of 0.5 mm flexural extension (previously determined to be non-destructive) [22]. The flexural load at 0.5 mm extension was recorded for each sample. Intact ulnae were similarly prepared and used as healthy controls.

2.5. MicroCT analysis

High resolution microCT was used to evaluate device degradation and new bone formation. Devices were scanned before implantation with a VivaCT40 (Scanco Medical AG, Bruttisellen, Switzerland) and 10.5 μm voxel size (55 kV, 72 μA). In addition, devices were scanned after 8 and 16 weeks ($n = 4$ per time point) using a SkyScan1172 (Bruker-MicroCT, Kontich, Belgium) scanner with a 10 μm voxel size, 79 kV tube potential and 125 μA tube current. 3D volumes of the scanned samples were generated from acquired 2D lateral projections using Recon software (Bruker-MicroCT, Kontich, Belgium). For analysis, scanned bone volumes were digitally reoriented using the SkyScan DataViewer software, and user-defined remaining Mg and corrosion product regions of interest were generated using the SkyScan CTAn software (version 1.13.5.1) as previously described [23,24]. Mg devices were segmented from surrounding soft and hard tissues based on the absorption coefficient (equivalent to mineral density) of remaining Mg and corrosion product. The relative X-ray absorption coefficients within each of these two layers are distinctly different, generating a clear interface between the two, as well as between the corroded product and background as previously described [23]. These interfaces were identifiable as inflection points within the distribution of mineral densities histogram from a region of interest including both remaining Mg and corrosion product. These inflection points were used to define thresholds for the Mg and corrosion product, and were verified by visual inspection.

Following segmentation, volume quantifications were obtained to evaluate device degradation and bone formation. Corrosion rate was calculated through the microCT-evaluated Mg volume loss using Eq. (1), where CR is corrosion rate in mm/yr, ΔV is change in Mg volume in mm^3 , A is surface area in mm^2 , and t is time in years [25]. Devices were considered in their entirety, and also divided into head and shaft regions with respective regions of interest defined. The head region was defined as any area of the screw above the bottom edge of the plate, while the shaft region was defined as any area of the screw below the bottom edge of the plate.

In addition to device volume change, new bone formation around the devices, as well as bone-device contact was assessed through microCT. New bone around the devices was defined as any bone above the bottom of the plate. Importantly, this region originally contained only muscle and soft tissue; therefore, any

bone observed within this region is newly formed. Bone contact throughout the screw shafts was calculated as the intersection surface area between Mg and bone using CTAn:

$$\text{CR} = \Delta V / (At) \quad (1)$$

2.6. Histological processing

Samples were formalin fixed and embedded in Technovit 9100 New[®] (Heraeus Kulzer, Hanau, Germany). Samples were sectioned and stained with Toluidine Blue to visualize bone morphology at the fracture site, device-tissue interface, and within areas of newly formed bone.

2.7. Statistical analysis

Statistical analysis was performed using IBM SPSS Statistics 19 (IBM, Armonk, NY). All groups were compared using student's t -test. For corrosion analysis, screw volumes were compared between two time points (0 and 8 weeks, $n = 8$ screws per time point). In addition, screw volumes were compared between the head and shaft regions (0 and 8 weeks, $n = 8$ screws per region). Plate volumes were similarly compared between two time points (0 and 8 weeks, $n = 2$ plates per time point). For mechanical testing analysis, healed ulnae were compared to healthy controls at 16 weeks ($n = 9$ ulnae per group). All graphical representations reflect mean \pm standard deviation.

3. Results

3.1. Mg devices did not cause adverse health events

All devices were well tolerated by the animals. Immediately following surgery, animals resumed normal movement and behavior, including weight bearing on both forearms.

3.2. Mg device underwent gradual degradation accompanied by corrosion product formation and gas formation

Initial evidence of device degradation was observed through subcutaneous gas pocket formation. Interestingly, subcutaneous gas pocket formation was not observed in all animals. Only two animals developed subcutaneous gas pockets over the implant site, which were easily removed with a sterile syringe without causing infection or interference with healing. Pockets consisted of gas without additional blood or fluid. Gas pocket formation was observed through 5 weeks post-operative. The largest number of removals, three, was performed during the second week, with all other weeks only requiring one removal each. No gas pocket formation was observed after 5 weeks post-operative.

High resolution microCT was used to study device degradation ($n = 8$ screws, $n = 2$ plates). Based on distinct material density differences, volumes of Mg and corrosion product were quantified separately. Volume quantification revealed a net loss of volume for Mg screws after 8 weeks. Mg volume was reduced by $4.41 \pm 0.49 \text{ mm}^3$ after 8 weeks. Meanwhile, $3.35 \pm 0.60 \text{ mm}^3$ of corrosion product was produced at the surface (Fig. 2A). Based on this change in Mg volume, the *in vivo* corrosion rate of our Mg screws was calculated to be $0.40 \pm 0.04 \text{ mm/year}$. Interestingly, corrosion behavior varied between different regions of the screws. After 8 weeks, the screw head region consisted of 47.09 ± 13.76 volume per cent of Mg, and 52.91 ± 13.76 volume per cent of corrosion product. In contrast, the screw shaft region consisted of 75.04 ± 3.34 volume per cent of Mg, and 24.96 ± 3.34 volume per cent of corrosion product (Fig. 2B). Similar to the screws, the Mg plate volume was

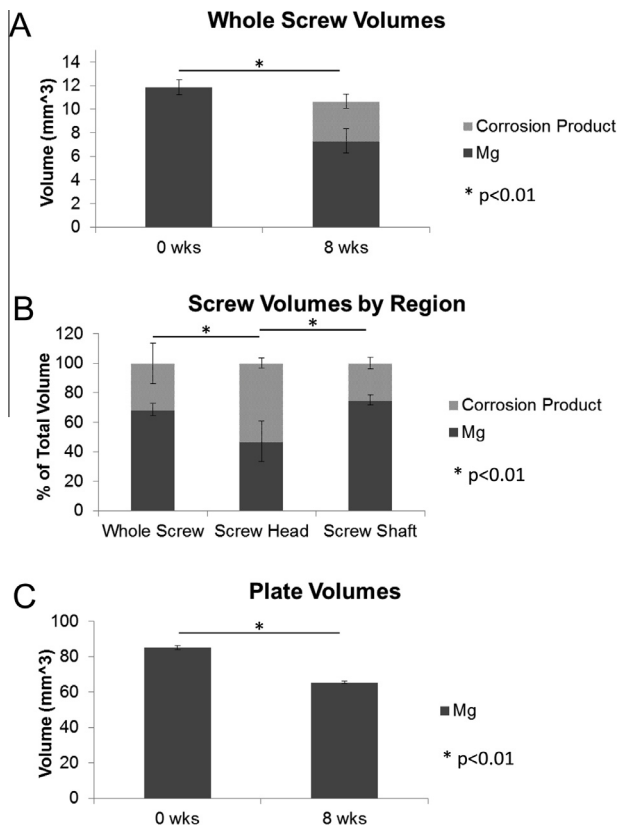


Fig. 2. Screw degradation after 8 weeks was assessed by volume quantification. Due to distinct density differences, Mg and corrosion product were quantified separately for a more detailed understanding of corrosion behavior. Volume quantification shows a Mg volume loss of $4.41 \pm 0.49 \text{ mm}^3$ after 8 weeks ($*p < 0.01$). In addition, $3.35 \pm 0.60 \text{ mm}^3$ of corrosion product was formed at the surface (A). Mg and corrosion product were calculated as percentages of total screw volume for the whole screw, the head region, and the shaft region at 8 weeks post-op. At this time point, Mg represented a significantly smaller percentage of total volume within the head region when compared to the shaft and whole screw (B, $*p < 0.01$). Concurrently, corrosion product represented a significantly greater percentage of total volume within the head region when compared to the shaft and whole screw (B, $*p < 0.01$). Plate volume was reduced by $19.57 \pm 0.66 \text{ mm}^3$ after 8 weeks (C, $*p < 0.01$).

also reduced after 8 weeks. Specifically, Mg plates corroded at a rate of $0.55 \pm 0.02 \text{ mm/year}$, resulting in $19.57 \pm 0.66 \text{ mm}^3$ of Mg volume loss after 8 weeks (Fig. 2C). Due to extensive corrosion product formation and integration with the surrounding tissues, accurate device volume quantification after 16 weeks was not possible. However, additional Mg volume loss and corrosion product production was observed.

3.3. Fracture healing was uninhibited by degrading Mg devices

Bi-weekly X-rays showed progressive healing throughout the study (Fig. 3). These observations were confirmed by microCT and histological staining after 8 and 16 weeks. After 8 weeks, fracture healing was observed as proximal and distal cortical bone union for most samples (Fig. 4A). After 16 weeks, more mature healing was observed, with full thickness cortical bone bridging at the fracture site (Fig. 4B). Histological staining showed normal bone morphology within these regions including osteocytes and osteoid (Fig. 4C–F).

3.4. Bone-device contact prevalent despite ongoing device degradation

Bone device contact was observed through microCT and histological staining. In the presence of ongoing corrosion, high levels

of bone-device contact were observed after 8 and 16 weeks *in vivo*. Areas of bone-device contact were more prevalent in slower degrading regions, such as around the plate and screw heads. New bone growth was often observed around the screw head and within the driver slot, with direct bone-device contact (Fig. 5). Bone device contact along screw shafts was quantified after 8 weeks, revealing over 25% of the screw shaft surface area in contact with bone.

3.5. Abundant bone growth observed over and around degrading Mg devices

New bone was formed over and around all Mg devices. This bone formation was observed throughout the study by X-ray, and was further assessed by microCT and histological staining after eight and 16 weeks. After 8 weeks, new bone partially covered all Mg devices (Fig. 6A–C). After 16 weeks, this new bone completely covered all Mg devices (Fig. 6D–F). MicroCT was used to quantify the amount of new bone formed over the fixation devices. A significant increase in overlying bone formation was observed from eight to 16 weeks ($p = 0.001$), with $100.20 \pm 33.80 \text{ mm}^3$ of new bone formed within this period (Fig. 6G).

3.6. Forearm structural properties maintained after 16 weeks

The relative structural properties of the healed ulnae were assessed by three point bend testing after 16 weeks. Bone overgrowth and degraded fixation devices were left in place for testing; therefore, results reflect the entire bone-device complex as it would be loaded *in vivo*. Bend test results revealed a slight, though not significant, increase in flexural load for healed ulnae fixed with Mg devices compared to intact ulna controls (Fig. 7).

4. Discussion

In the present study, we assessed the efficacy of degradable Mg fixation plates and screws in a loaded ulna fracture model. This model has been used to study bone repair and effects of implants and therapeutic agents on fracture healing [24–26]. Previously, our group performed a pilot study evaluating the biological effect of Mg plates and screws. This study revealed abundant new bone formation around the degrading Mg devices, suggesting a connection between Mg degradation and bone formation. To further explore the effect of Mg on fracture healing and bone formation, we have conducted a thorough investigation of 99.9% Mg fixation plates and screws. We hypothesized that these degradable devices would facilitate fracture healing, while stimulating local bone formation.

As Mg degrades, hydrogen gas is produced. Depending on the implant's local environment and available blood flow, this gas may be cleared from the implant site without accumulation. However, rapid corrosion rate and/or insufficient gas removal may lead to accumulation. Several studies have documented gas cavity formation associated with Mg degradation [10,27]. Kraus et al. used microCT to study gas formation and Mg pin degradation in rat femora [17]. They showed gas formation closely followed Mg volume reduction. Furthermore, they showed that gas was largely resorbed by the surrounding tissue, and did not cause adverse effects on bone healing. In the present study, six gas pockets from two animals were observed over the course of the study, indicating that most gas released during device degradation was efficiently cleared from the implant site. Furthermore, the observed gas accumulation did not disrupt fracture healing, bone formation, or surrounding tissue health. It is important to note however, that reducing gas pocket formation is necessary for clinical translation.

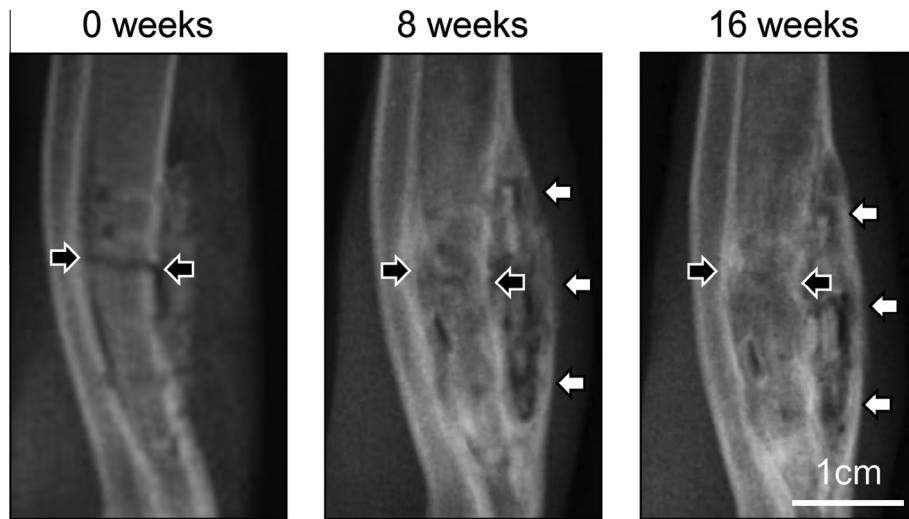


Fig. 3. X-rays showing fracture healing and bone over growth progression. Fracture healing was observed by 8 weeks with further maturation by 16 weeks post-operative (black arrows). In addition, new bone was formed over the entire fixation device. Partial bone covering was observed by 8 weeks, with complete covering occurring by 16 weeks post-operative (white arrows).

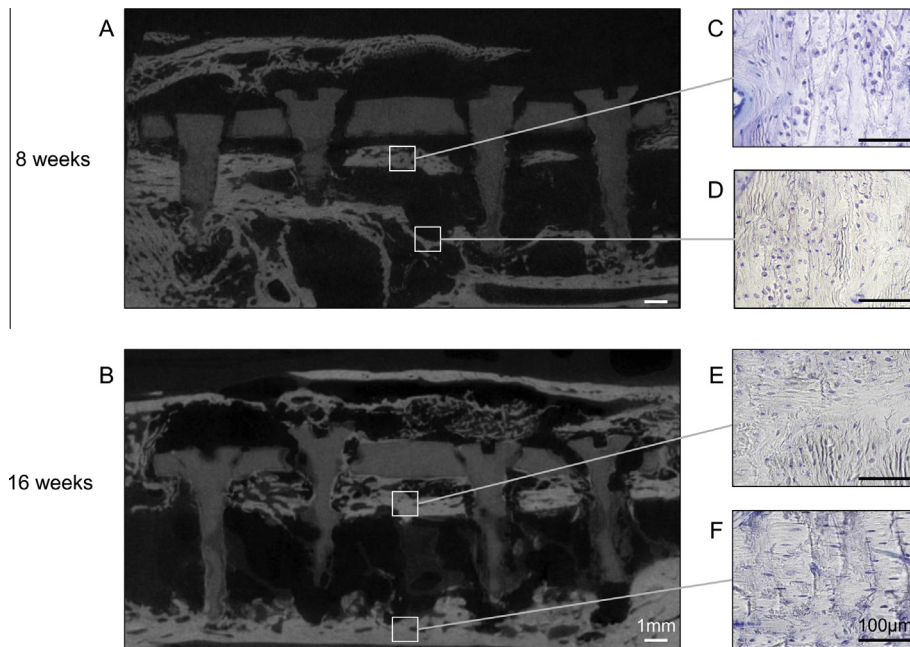


Fig. 4. MicroCT and histological staining show further detail of fracture healing. MicroCT slices show cortical bone union after 8 weeks (A) with further maturation after 16 weeks (B). High magnification images of Toluidine stained sections show normal bone morphology within the healed cortical bones at the fracture site after 8 (C and D) and 16 weeks (E and F).

One way to achieve this could be through grain refinement, as has been previously demonstrated with Mg alloy LAE442 [28]. In the study by Ullmann et al., LAE442 rods with varying grain sizes were implanted into the medullary cavity of New Zealand white rabbits and assessed over 6 months. Their results demonstrated that grain size reduction provided slower corrosion and improved clinical tolerance. It is likely that grain refinement of the pure Mg used in the present study (average grain size $36.9 \mu\text{m}$) would provide similar corrosion improvements for instance, through mechanisms such as improved passive film formation due to increased activity of reduced grain size area, and consequently, better adhesion due to increased grain boundary density [29]. As a result, gas pocket formation may be likely reduced.

In addition to hydrogen, degrading Mg produces corrosion product on its surface [10,30]. The materials properties of the remaining Mg and corrosion product are expectedly not equal, and therefore do not provide equal contributions to device function. For these reasons, we assessed device degradation in terms of Mg volume loss and corrosion product volume gain. We observed a net volume loss for all devices, with considerable corrosion product formation. Interestingly, we observed a greater corrosion rate for the plates than the screws (0.55 ± 0.02 and 0.40 ± 0.04 mm/year, respectively). We hypothesize that this difference is attributed to the devices' local environment. Unlike the screws, which were largely contained within bone, the plates were initially covered by muscle. This tissue has a higher water content and blood

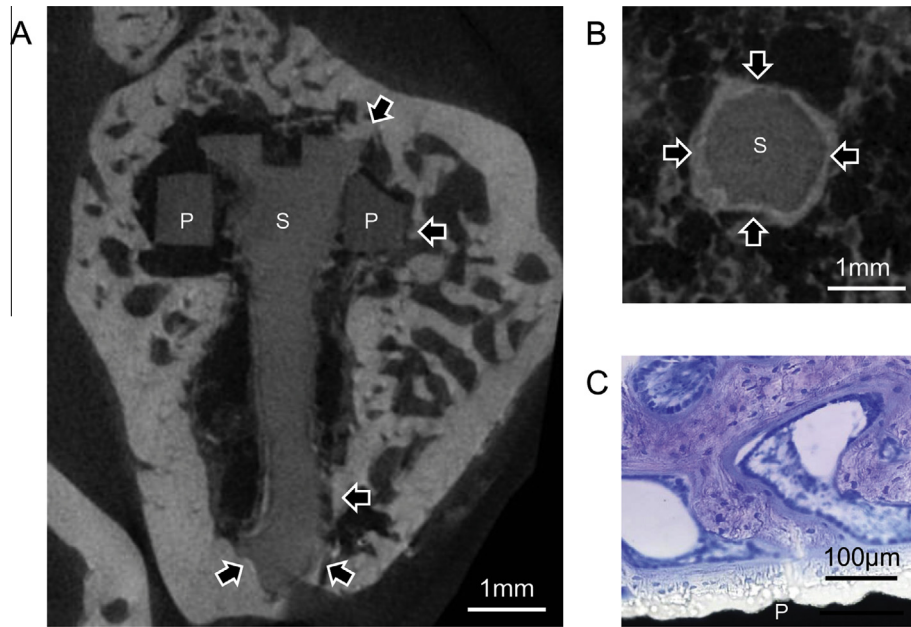


Fig. 5. Areas of bone-device contact observed after eight and 16 weeks. Interfaces of Mg devices (lower density, darker) and bone (higher density, brighter) were observed through microCT. A longitudinal slice of a Mg plate (P) and screw (S) show areas of bone contact around the screw head, shaft, and plate edge (A). A transverse slice of a Mg screw shaft (S) shows bone contact around screw perimeter after 16 weeks (B). Toluidine Blue shows bone morphology at bone-plate (P) interface after 8 weeks (C).

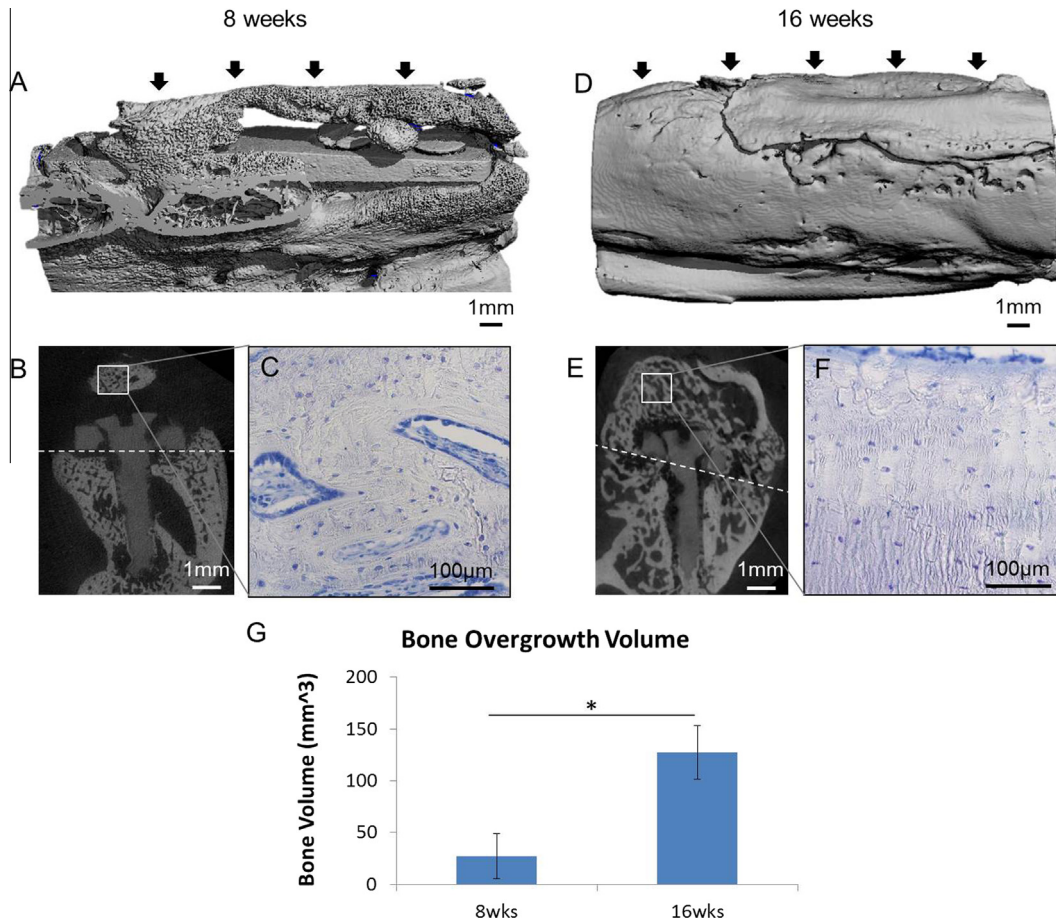


Fig. 6. Bone overgrowth (black arrows) around degrading Mg devices. MicroCT 3D rendering after 8 weeks shows partial bone overgrowth around the degrading Mg device (A). By 16 weeks, bone overgrowth completely covered all devices (D). X-ray slices from microCT scanning highlight bone overgrowth over screws after 8 (B) and 16 weeks (E). Toluidine Blue histological stain shows normal bone morphology with osteocytes and osteoid within the newly formed bone (C and F). New bone overgrowth was quantified using microCT. Conservatively, bone above the plate baseline (marked with a white dotted line) was identified as new bone. A significant increase in bone was observed from 8 to 16 weeks (G, **p* < 0.01).

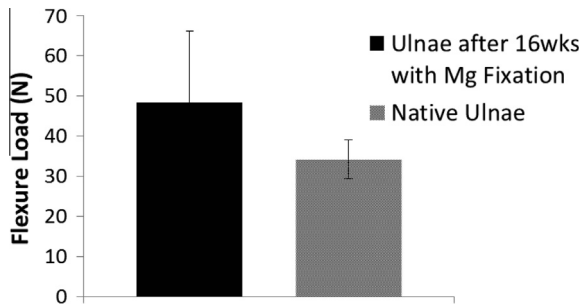


Fig. 7. Bend test results. Bend testing was performed on ulnae after 16 weeks and compared to healthy, un-fractured controls. Fixation devices and bone overgrowth were not removed for testing. Student's *t*-test revealed no significant differences between healed ulnae and healthy controls.

flow than bone, and therefore likely accelerated plate corrosion [27].

Interestingly, we also observed differences in corrosion behavior between screw regions. Specifically, our data suggest that corrosion was enhanced for screw heads compared to shafts. Similar observations of varied degradation behavior for Mg screws have been previously reported [10,31–33]. For instance, Willbold et al. implanted Mg alloy AZ31 screws into the hip bone of sheep. After 3 and 6 months, they observed accelerated corrosion of screw heads (surrounded by soft tissue) when compared to screw shafts (surrounded by bone) [31]. Uniquely, our screws were tested as part of a fixation system, and therefore screw heads were in contact with the overlying soft tissue, as well as the fixation plate. Shearing of these components, as well as compression during loading, likely contributed to corrosion within the head region [10,34,35]. A similar effect of compression on corrosion was shown by Denkena et al. using LAE442 rods *in vitro*. They observed an increased corrosion rate with compressive stress and a decreased corrosion rate with tensile stress [36]. Despite these observations of accelerated corrosion, all devices remained in place and provided sufficient stabilization throughout the study. Furthermore, high levels of bone-device contact were observed, revealing osteointegration of the devices.

In the presence of ongoing device corrosion, fracture healing remained uninhibited, and cortical bone union matured throughout the study. These observations are in accordance with our previous study which demonstrated healing of similar rabbit ulna fractures after 4 weeks. In the present study, we observed more mature healing after 8 weeks, which is consistent with the reported healing time of rabbit fractures [25]. These results demonstrate the ability of Mg fixation devices to facilitate physiological healing and long-term remodeling in a loaded fracture environment. Importantly, this reflects a unique advantage of Mg alloys over resorbable polymer devices, which are often not suitable for load bearing applications.

Uniquely, Mg devices have the potential to not only facilitate fracture healing, but also enhance bone formation. Several studies have highlighted this potential by showing increased mineral apposition, bone mass, and bone mineral density around Mg implants in bone [16,19,20,37]. For instance, in a notable study by Witte et al., degradable Mg and polymeric implants were placed in the intramedullary space of guinea pig femora [16]. After six and 18 weeks, they observed a significant increase in mineralization for all groups with Mg implants when compared to polymeric controls. Similar results were observed with fast corroding Mg implants in rabbit femur [18]. These results highlighted the potential of degrading Mg implants to elicit a positive bone growth response, establishing their potential as strong candidates for orthopedic implants. To our knowledge, however, there have been

no reported investigations of Mg's ability to encourage bone formation in a traumatic fracture environment. In the present study, we observed abundant bone formation over and around all degrading Mg devices. This bone formation occurred over the devices, where periosteal and muscle tissue layers are typically present, suggesting the ability of Mg-ion release from device degradation to affect osteoblastic cell differentiation. This observation is in accordance with our previous study in which *de novo* bone formation was observed around Mg plates and screws after 4 weeks [21], as well as a previous report of LAE442 screws and plates implanted in intact rabbit tibia [36]. With the present study, we have confirmed our pilot study observations, and demonstrated that prolonged exposure to Mg degradation can cause progressive bone formation. This bone formation is not typically seen with resorbable polymer or permanent metal devices, and therefore highlights a unique advantage of Mg fixation devices. In this manner, the degrading fixation device is gradually replaced by bone, without compromising fracture healing.

The mechanism of this bone growth is not yet fully understood, though some *in vitro* studies have been conducted to elucidate mechanisms of Mg's effect on bone cells [38]. We hypothesized that as these devices degrade, Mg is released, and local cells are stimulated to form bone (Fig. 8). This effect has been demonstrated *in vitro* by exposing cells to Mg ion and assessing their osteogenic response [38,39]. In addition, various *in vivo* models have also shown a beneficial effect of Mg degradation on bone [16,19,20,37]. Considering the location of the newly formed bone observed in the present study, it is likely that the periosteum served as a cell source for osteogenic differentiation (Fig. 8). Cells within this tissue layer, including osteoblasts and pluripotent mesenchymal stem cells, are known to facilitate bone growth and repair [40,41]. It is possible that Mg released from our degrading devices stimulated stem cells within the periosteum to initiate bone formation over the devices. This hypothesis is consistent with previous work by Bondarenko et al. which demonstrated that fast corroding Mg implants enhanced expression of osteocalcin and osteopontin in surrounding bone tissue [42]. It is likely that the bone formation observed in the present study then continued as device degradation, and subsequent Mg release, persisted over time.

We hypothesize that this new bone contributes to the structural properties of the ulna, helps provide stabilization, and further facil-

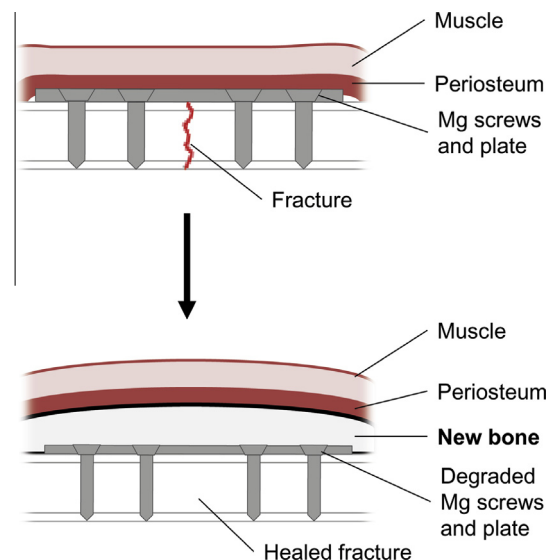


Fig. 8. Schematic of proposed mechanism for Mg stimulated bone formation.

itates weight-bearing activity during healing. Through three point bend testing, we observed a similar flexure load response of the healed ulnae when compared to healthy, un-fractured controls. Importantly, these results reveal that the structural properties of healed bone are similar to native ulnae, and that functional regeneration has occurred.

5. Conclusion

In the present study we assessed the efficacy of degradable Mg fixation plates and screws in a loaded rabbit ulna model. We have demonstrated that Mg device degradation does not inhibit fracture healing and enhances bone formation around the devices. Furthermore, we observed *de novo* bone formation above the devices, suggesting a role of Mg in cell differentiation and bone growth. To our knowledge, this is the first study to show the effect of Mg screws and plates on a loaded fracture model. These data support the potential use of pure Mg as fracture fixation devices.

Acknowledgements

This study was supported by the National Science Foundation Engineering Research Center for Revolutionizing Metallic Biomaterials (Grant 0812348), the Commonwealth of Pennsylvania (SAP4100061184), the University of Pittsburgh's Center for Craniofacial Regeneration, and PNK acknowledges the Edward R. Weidlein Chair Professorship funds from the Swanson School of Engineering, University of Pittsburgh. The authors would like to thank Andrew Holmes (University of Pittsburgh) for device fabrication, Dr. Michael Epperly (University of Pittsburgh) for device sterilization, and Dr. Alejandro Almarza (University of Pittsburgh) for assistance with mechanical testing.

Appendix A. Figures with essential color discrimination

Certain figures in this article, particularly Figs. 1–8 are difficult to interpret in black and white. The full color images can be found in the on-line version, at <http://dx.doi.org/10.1016/j.actbio.2015.02.010>.

References

- [1] Stevens B, Yang Y, Mohandas A, Stucker B, Nguyen KT. A review of materials, fabrication methods, and strategies used to enhance bone regeneration in engineered bone tissues. *J Biomed Mater Res B Appl Biomater* 2008;85B:573–82.
- [2] Orthopedic Network News 2011, Trauma Update. 2011.
- [3] Chou DT, Hong D, Saha P, Ferrero J, Lee B, Tan Z, et al. In vitro and in vivo corrosion, cytocompatibility and mechanical properties of biodegradable Mg–Y–Ca–Zr alloys as implant materials. *Acta Biomater* 2013;9:8518–33.
- [4] Pietak A, Mahoney P, Dias GJ, Staiger MP. Bone-like matrix formation on magnesium and magnesium alloys. *J Mater Sci – Mater Med* 2008;19:407–15.
- [5] Puleo DA, Huh WW. Acute toxicity of metal ions in cultures of osteogenic cells derived from bone marrow stromal cells. *J Appl Biomater* 1995;6:109–16.
- [6] Jacobs JJ, Gilbert JL, Urban RM. Corrosion of metal orthopaedic implants. *J Bone Joint Surg Am* 1998;80:268.
- [7] Staiger MP, Pietak AM, Huadmai J, Dias G. Magnesium and its alloys as orthopedic biomaterials: a review. *Biomaterials* 2006;27:1728–34.
- [8] Hanson B, van der Werken C, Stengel D. Surgeons' beliefs and perceptions about removal of orthopaedic implants. *BMC Musculoskelet Disord* 2008;9:73.
- [9] Busam ML, Esther RJ, Obremsky WT. Hardware removal: indications and expectations. *J Am Acad Orthop Surg* 2006;14:113–20.
- [10] Zheng YF, Gu XN, Witte F. Biodegradable metals. *Mater Sci Eng R Rep* 2014;77:1–34.
- [11] Böstman O, Hirvensalo E, Mäkinen J, Rokkanen P. Foreign-body reactions to fracture fixation implants of biodegradable synthetic polymers. *J Bone Joint Surg Br* 1990;72:592.
- [12] Weiler A, Helling HJ, Kirch U, Zirbes TK, Rehm KE. Foreign-body reaction and the course of osteolysis after polyglycolide implants for fracture fixation: experimental study in sheep. *J Bone Joint Surg Br* 1996;78:369–76.
- [13] Walker J, Shadanbaz S, Woodfield TB, Staiger MP, Dias GJ. Magnesium biomaterials for orthopedic application: a review from a biological perspective. *J Biomed Mater Res Part B, Appl Biomater* 2014.
- [14] Witte F. The history of biodegradable magnesium implants: a review. *Acta Biomater* 2010;6:1680–92.
- [15] Hong D, Saha P, Chou DT, Lee B, Collins BE, Tan Z, et al. In vitro degradation and cytotoxicity response of Mg–4% Zn–0.5% Zr (ZK40) alloy as a potential biodegradable material. *Acta Biomater* 2013;9:8534–47.
- [16] Witte F, Kaese V, Haferkamp H, Switzer E, Meyer-Lindenberg A, Wirth CJ, et al. In vivo corrosion of four magnesium alloys and the associated bone response. *Biomaterials* 2005;26:3557–63.
- [17] Kraus T, Fischerauer SF, Hänzli AC, Uggowitzer PJ, Löffler JF, Weinberg AM. Magnesium alloys for temporary implants in osteosynthesis: in vivo studies of their degradation and interaction with bone. *Acta Biomater* 2012;8:1230–8.
- [18] Willbold E, Kalla K, Bartsch I, Bohe K, Brauneis M, Remennik S, et al. Biocompatibility of rapidly solidified magnesium alloy RS66 as a temporary biodegradable metal. *Acta Biomater* 2013;9:8509–17.
- [19] Janning C, Willbold E, Vogt C, Nellesen J, Meyer-Lindenberg A, Windhagen H, et al. Magnesium hydroxide temporarily enhancing osteoblast activity and decreasing the osteoclast number in peri-implant bone remodelling. *Acta Biomater* 2010;6:1861–8.
- [20] Yang JX, Cui FZ, Lee IS, Zhang Y, Yin QS, Xia H, et al. In vivo biocompatibility and degradation behavior of Mg alloy coated by calcium phosphate in a rabbit model. *J Biomater Appl* 2012;27:153–64.
- [21] Chaya A, Yoshizawa S, Verdellis K, Noorani S, Costello BJ, Sfeir C. Fracture healing using degradable magnesium fixation plates and screws. *J Oral Maxillofac Surg* 2015;73:295–305.
- [22] Zaky SH, Lee KW, Gao J, Jensen A, Close J, Wang Y, et al. Poly(glycerol sebacate) elastomer: a novel material for mechanically loaded bone regeneration. *Tissue Eng Part A* 2014;20:45–53.
- [23] Witte F, Fischer J, Nellesen J, Vogt C, Vogt J, Donath T, et al. In vivo corrosion and corrosion protection of magnesium alloy LAE442. *Acta Biomater* 2010;6:1792–9.
- [24] Luppen CA, Blake CA, Ammirati KM, Stevens ML, Seeherman HJ, Wozney JM, et al. Recombinant Human bone morphogenetic protein-2 enhances osteotomy healing in glucocorticoid-treated rabbits. *J Bone Miner Res* 2002;17:301–10.
- [25] Mills LA, Simpson AH. In vivo models of bone repair. *J Bone Joint Surg Br* 2012;94:865–74.
- [26] Schatzker J, Chapman M, Ha'Eri GB, Fornasier VL, Sumner-Smith G, Williams C. The effect of calcitonin on fracture healing. *Clin Orthop Relat Res* 1979:303–6.
- [27] Witte F, Hort N, Vogt C, Cohen S, Kainer KU, Willumeit R, et al. Degradable biomaterials based on magnesium corrosion. *Curr Opin Solid State Mater Sci* 2008;12:63–72.
- [28] Ullmann B, Reifenrath J, Seitz JM, Bormann D, Meyer-Lindenberg A. Influence of the grain size on the in vivo degradation behaviour of the magnesium alloy LAE442. *Proc Inst Mech Eng [H]* 2013;227:317–26.
- [29] Ralston KD, Birbilis N. Effect of grain size on corrosion: a review. *Corrosion* 2010;66:075005–75013.
- [30] Bowen PK, Drelich J, Goldman J. Magnesium in the murine artery: probing the products of corrosion. *Acta Biomater* 2014;10:1475–83.
- [31] Willbold E, Kaya AA, Kaya RA, Beckmann F, Witte F. Corrosion of magnesium alloy AZ31 screws is dependent on the implantation site. *Mater Sci Eng B* 2011;176.
- [32] Erdmann N, Angrisani N, Reifenrath J, Lucas A, Thorey F, Bormann D, et al. Biomechanical testing and degradation analysis of MgCa0.8 alloy screws: a comparative in vivo study in rabbits. *Acta Biomater* 2011;7:1421–8.
- [33] Xu L, Yu G, Zhang E, Pan F, Yang K. In vivo corrosion behavior of Mg–Mn–Zn alloy for bone implant application. *J Biomed Mater Res, Part A* 2007;83A:703–11.
- [34] Zhang S, Zhang X, Zhao C, Li J, Song Y, Xie C, et al. Research on an Mg–Zn alloy as a degradable biomaterial. *Acta Biomater* 2010;6:626–40.
- [35] Wang Q, Tan L, Xu W, Zhang B, Yang K. Dynamic behaviors of a Ca–P coated AZ31B magnesium alloy during in vitro and in vivo degradations. *Mater Sci Eng, B* 2011;176:1718–26.
- [36] Denkena B, Köhler J, Stieghorst J, Turger A, Seitz J, Fau DR, et al. Influence of stress on the degradation behavior of Mg LAE442 implant systems. *Procedia CIRP* 2013, p. 189–95.
- [37] Witte F, Ulrich H, Palm C, Willbold E. Biodegradable magnesium scaffolds. Part II: peri-implant bone remodeling. *J Biomed Mater Res, Part A* 2007;81:757–65.
- [38] Yoshizawa S, Brown A, Barchowsky A, Sfeir C. Magnesium ion stimulation of bone marrow stromal cells enhances osteogenic activity, simulating the effect of magnesium alloy degradation. *Acta Biomater* 2014;10:2834–42.
- [39] Yun Y, Dong Z, Yang D, Schulz MJ, Shanov VN, Yarmolenko S, et al. Biodegradable Mg corrosion and osteoblast cell culture studies. *Mater Sci Eng, C* 2009;29:1814–21.
- [40] Colnot C, Zhang X, Knothe Tate ML. Current insights on the regenerative potential of the periosteum: molecular, cellular, and endogenous engineering approaches. *J Orthop Res* 2012;30:1869–78.
- [41] Malizos KN, Papatheodorou LK. The healing potential of the periosteum: molecular aspects. *Injury* 2005;36:S13–9.
- [42] Bondarenko A, Angrisani N, Meyer-Lindenberg A, Seitz JM, Waizy H, Reifenrath J. Magnesium-based bone implants: immunohistochemical analysis of peri-implant osteogenesis by evaluation of osteopontin and osteocalcin expression. *J Biomed Mater Res Part A* 2014;102:1449–57.